Original Article

MOLECULAR METABOLISM

Lysine tRNA fragments and miR-194-5p co-regulate hepatic steatosis via β-Klotho and perilipin 2

Yonat Tzur [1], Katarzyna Winek [1,2], Nimrod Madrer [1], Serafima Dubnov [1,2], Estelle R. Bennett [1], David S. Greenberg [1], Geula Hanin [1,5], Asaad Gammal [3], Joseph Tam [3], Isaiah T. Arkin [1], Iddo Paldor [4], Hermona Soreq [1,2,*]

ABSTRACT

Objective: Non-alcoholic fatty liver disease (NAFLD) involves hepatic accumulation of intracellular lipid droplets via incompletely understood processes. Here, we report distinct and cooperative NAFLD roles of LysTTT-5′tRF transfer RNA fragments and microRNA miR-194-5p.
Methods: Combined use of diet induced obese mice with human-derived oleic acid-exposed Hep G2 cells revealed new NAFLD roles of LysTTT-5′tRF and miR-194-5p.
Results: Unlike lean animals, dietary-induced NAFLD mice showed concurrent hepatic decrease of both LysTTT-5′tRF and miR-194-5p levels, which were restored following miR-132 antisense oligonucleotide treatment which suppresses hepatic steatosis. Moreover, exposing human-derived Hep G2 cells to oleic acid for 7 days co-suppressed miR-194-5p and LysTTT-5′tRF levels while increasing lipid accumulation. Inversely, transfecting fattened cells with a synthetic LysTTT-5′tRF mimic elevated mRNA levels of the metabolic regulator β-Klotho while decreasing triglyceride amounts by 30% within 24 h. In contradistinction, antisense suppression of miR-194-5p induced accumulation of its novel target, the NAFLD-implicated lipid droplet-coating PLIN2 protein. Further, two out of 15 steatosis-alleviating screened drug-repurposing compounds, Danazol and Latanoprost, elevated miR-194-5p or LysTTT-5′tRF levels.
Conclusion: Our findings highlight the different yet complementary roles of miR-194-5p and LysTTT-5′tRF and offer new insights into the complex roles of small non-coding RNAs and the multiple pathways involved in NAFLD pathogenesis.

Keywords KLB; LysTTT-5′tRFs; microRNAs; miR-194-5p; NAFLD; PLIN2; tRFs

1. INTRODUCTION

Non-alcoholic fatty liver disease (NAFLD), also referred to as metabolic dysfunction-associated steatotic liver disease (MASLD), is the leading cause of chronic liver disease and one of the most common liver disorders worldwide. NAFLD/MASLD involves hepatic accumulation of lipid droplets (LDs), which are composed of a neutral lipid core surrounded by a lipid monolayer and decorated with a repertoire of specific proteins [1,2]. NAFLD begins with simple steatosis, which may progress to non-alcoholic steatohepatitis (NASH) with subsequent higher risk of cirrhosis and hepatocellular carcinoma [3]. Often considered as the hepatic manifestation of metabolic syndrome, NAFLD is associated with obesity, hypertension, dyslipidemia, central adiposity, insulin resistance, and diabetes [4,5]. Due to its growing prevalence, there is a need to explore the underlying mechanisms of NAFLD development and progression, and seek novel routes for treatment. Since LD accumulation in hepatocytes is the primary characteristic of NAFLD, great efforts have been invested in research aiming to understand LD formation, regulation and contributions to NAFLD progression. LDs are coated by LD-associated proteins such as the perilipins (PLINs), which take part in LD formation, stabilization, and trafficking [6,7]. Of those, PLIN2 is the major hepatic LD protein. Its

[1]The Silberman Institute of Life Sciences, The Hebrew University of Jerusalem, Edmond J. Safra Campus, Jerusalem, Israel [2]The Edmond and Lily Safra Center of Brain Science, The Hebrew University of Jerusalem, Edmond J. Safra Campus, Jerusalem, Israel [3]Obesity and Metabolism Laboratory, The Institute for Drug Research, School of Pharmacy, Faculty of Medicine, The Hebrew University of Jerusalem, Jerusalem, Israel [4]Shaare Zedek Medical Center, The Neurosurgery Department, Main Building, 10th Floor, 12 Shmu'el Bait Street, Jerusalem, 9103102 Israel

[5] Current address: Department of Genetics, University of Cambridge, Cambridge, United Kingdom.

*Corresponding author. The Silberman Institute of Life Sciences, The Hebrew University of Jerusalem, Edmond J. Safra Campus, Jerusalem, Israel. E-mail: hermona.soreq@mail.huji.ac.il (H. Soreq).

Abbreviations: ASO, antisense oligonucleotide; BA, bile acid; CYP7A, cholesterol 7a-hydroxylase; DE, differential expression; DIO, diet-induced obesity; FGFR, fibroblast growth factor receptor; FXR, farnesoid X receptor; KLB, β-Klotho; LD, lipid droplet; MASLD, metabolic dysfunction-associated steatotic liver disease; miR, microRNA; NAFLD, non-alcoholic fatty liver disease; NASH, non-alcoholic steatohepatitis; OA, oleic acid; PLINs, perilipins; RCD, regular chow diet; RNA-seq, RNA sequencing; sncRNA, small non-coding RNA; tRFs, transfer RNA fragments

Received August 31, 2023 • Revision received November 20, 2023 • Accepted December 17, 2023 • Available online 22 December 2023

https://doi.org/10.1016/j.molmet.2023.101856

levels correlate with steatosis degree [6,8], and Plin2-deficient mice are NAFLD-resistant and display reduced hepatic triglycerides [9,10]. NAFLD pathology has been suggested to involve crosstalk between the liver, gut and adipose tissue [11,12]. A significant gut-derived signal that affects adipose tissue and liver response in NAFLD is the fibroblast growth factor (FGF) 15/19 and its receptor system [13]. FGF19 (FGF15 in the mouse), a member of the FGF19 subfamily along with FGF21 and FGF23, is secreted from the intestine and transported to the liver. There, it binds the fibroblast growth factor receptor-4 (FGFR4) assisted by the β-Klotho (KLB) co-receptor, to regulate bile acid (BA) synthesis and homeostasis, which are involved in NAFLD pathogenesis [14,15]. Thanks to its combined contributions in the liver, gut, and adipose tissue, and since KLB is a fundamental component that is essential for the complex activation of FGFR and the intracellular downstream responses of FGF signaling [16,17], KLB and its related proteins have emerged as promising targets for treating NAFLD [18].

Small non-coding RNAs (sncRNAs) have also been proposed to be causally involved in NAFLD's initiation and progression. These include microRNAs (miRs), small (∼22 nucleotides) regulators of gene expression that bind protein-coding mRNA transcripts, silence them post-transcriptionally [19], and regulate numerous biological processes including lipid metabolism, inflammation, and oxidative stress [20–22]. However, while several miRs were implicated in NAFLD pathophysiology [23–25], neither their routes of action nor their complete impact have fully been clarified.

The recently re-discovered transfer RNA fragments (tRFs) include active elements with miR-like capacities [26,27], generated by nucleolytic processing of intact tRNAs of nuclear and/or mitochondrial genome origins. Specific tRFs were found to be causally involved in the surveillance of cell proliferation, regulation of gene expression, RNA processing, tumor suppression and neurodegeneration [28–31], but the potential roles of tRFs in NAFLD remain unknown.

To study the involvement of miRs and tRFs in NAFLD, we have utilized a murine model previously developed in our laboratory in which diet-induced obese (DIO) mice were treated with an oligonucleotide targeting miR-132. While obese mice exhibited significant hepatic steatosis, with elevated serum triglycerides and LDL/VLDL, mice treated with an antisense oligonucleotide targeting mmu-miR-132-3p (termed AM132) inversely exhibited a reversal of the fatty liver phenotype [25]. We initiated the current study by performing small RNA sequencing of hepatic tissue from these mice following treatment with AM132 or a control molecule, and combined this with further experiments in human-derived Hep G2 cells to test the relevance of our findings for the human liver. In each of these systems we discovered a novel route, whereby complementary yet distinct actions of specific miRs and tRFs emerged as beneficial joint forces for NAFLD arrest.

2. RESULTS

2.1. miR-194-5p and LysTTT-originated tRFs decline jointly in a murine fatty liver model

Liver tissues of lean regular chow diet (RCD) and DIO mice treated with AM132 or AM608 (a control antisense targeting the primate-specific hsa-miR-608 and hereafter termed Ctrl) [25] were subjected to small RNA-seq (Figure 1A, Supp. materials and methods). Principal component analysis (PCA) segregating the levels of distinct treatment-specific patterns in AM132 compared to Ctrl mice revealed clustering of miRs by treatment (Figure 1B). Differential expression (DE) analysis revealed altered profiles of liver-expressed miRs (Figure 1D) in DIO mice with the hyperlipidemic phenotype vs Ctrl mice, including 34 upregulated and 47 downregulated miRs. PCA analysis of tRFs also revealed clustering according to treatment (Figure 1C) with DE expression of 13 upregulated and 5 downregulated tRFs (Figure 1E). Predictably, the AM132 anti-steatotic treatment downregulated miR-132-3p in AM132 mice (log2FoldChange = −12.3, padj = 4.6e-33). This was accompanied by altered levels of miR-122-5p, miR-148a-5p, miR-192-5p, let-7g-5p, let-7f-5p, miR-21a-5p, miR-99a-5p, miR-26a-5p, miR-194-5p, and miR-30a-5p, which were the top 10 DE miRs, based on their log2fold change and mean expression (count change [32]) (Figure 1D, Supp. Table 1). Notably, several of these miRs, including miR-122-5p, miR-21a-5p, and miR-192-5p, are known to be NAFLD-related [24,33]. Moreover, KEGG pathway analysis of the predicted targets [34] of all DE miRs showed "fatty acid metabolism" as the top affected pathway (p = 1.01E-17), indicating involvement of the identified miRs in the processes leading to liver fat accumulation (Figure 1F, Supp. Table 2). In comparison, the 18 DE tRFs originated from nuclear alanine, lysine, and histidine-carrying tRNA genes (Supp. Table 3). The top 10 DE molecules by count change measure included four alanine tRNA-derived fragments: 3′ tDR-55:76-Ala-CGC-1-M4, 5′ tDR-1:19-Ala-AGC-4-M7, 3′ tDR-55:76-Ala-CGC-3-M2, and 5′ tDR-1:25-Ala-AGC-4-M7; two lysine-tRNA-derived fragments: 5′ tDR-1:18-Lys-TTT-3-M2, 5′ tDR-1:21-Lys-TTT-3-M2; and one each from serine, arginine, histidine and glycine tRNAs: 5'tDR-1:16-Ser-AGA-1-M7, 5′ tDR-1:20-Arg-TCT-1, i-tDR-2:31-His-GTG-1, and 3′ tDR-55:76-Gly-TCC-1-M3, respectively (Figure 1E).

NAFLD's occurrence and persistence is often linked to altered brain activities, especially in the hypothalamus [35,36]. Therefore, we tested whether the AM132 treatment also affects hypothalamic small RNAs, by subjecting hypothalamic tissues from our NAFLD DIO mice to small RNA-seq. However, no tRFs, and only two miRs, were DE between the groups (Supp. Figure 1), suggesting that the effects of systemic AM132 treatment were limited to the liver.

2.2. PLIN2 is elevated in steatotic Hep G2 and in DIO mice

To investigate the relevance of selected regulatory sncRNAs in the mouse NAFLD model to liver pathophysiology in humans, we exposed human liver-derived hepatocellular carcinoma Hep G2 cells to 0.5 mM oleic acid (OA). Predictably, this triggered dose-dependent lipid accumulation [37], which was visualized by staining the cells with Nile Red (Figure 2A), a lipophilic compound that binds neutral lipids (mainly triglycerides and cholesteryl esters) in the core of LDs. This accumulation was also quantified by spectrophotometric measurement of Nile Red (Figure 2B), normalized to DAPI signal as reflecting cell number (see Supplementary Materials and Methods for details). Importantly, the observed lipid accumulation was accompanied by elevated mRNA and protein levels of the LD-coating perilipin 2 (PLIN2) (Figure 2C, D), which is the most enriched LD-coating protein in the liver, and the levels of which correlate with those of stored triglycerides [6]. Seeking molecular links, we quantified the levels of liver-expressed PLINs in our RCD and AM132 or Ctrl treated DIO mice. Notably, Plin2, Plin3, and Plin5 mRNA levels were all upregulated in DIO compared to RCD mice, but AM132-treatment led to decline of Plin2 levels alone compared to Ctrl mice, by ∼40% (Figure 2E). To further confirm the reduction in Plin2 we measured its protein levels in a subset of samples from each group. Indeed, PLIN2 protein levels were elevated in the DIO compared to RCD mice, with a ∼30% decrease in the AM132 compared to the Ctrl mice (Figure 2F–G).

2.3. miR-194-5p directly targets PLIN2

That AM132-treated mice showed lower Plin2 mRNA as well as protein levels than Ctrl mice could reflect either decreased steatosis and resultant reduced presence of lipid droplet-coating proteins, and/or

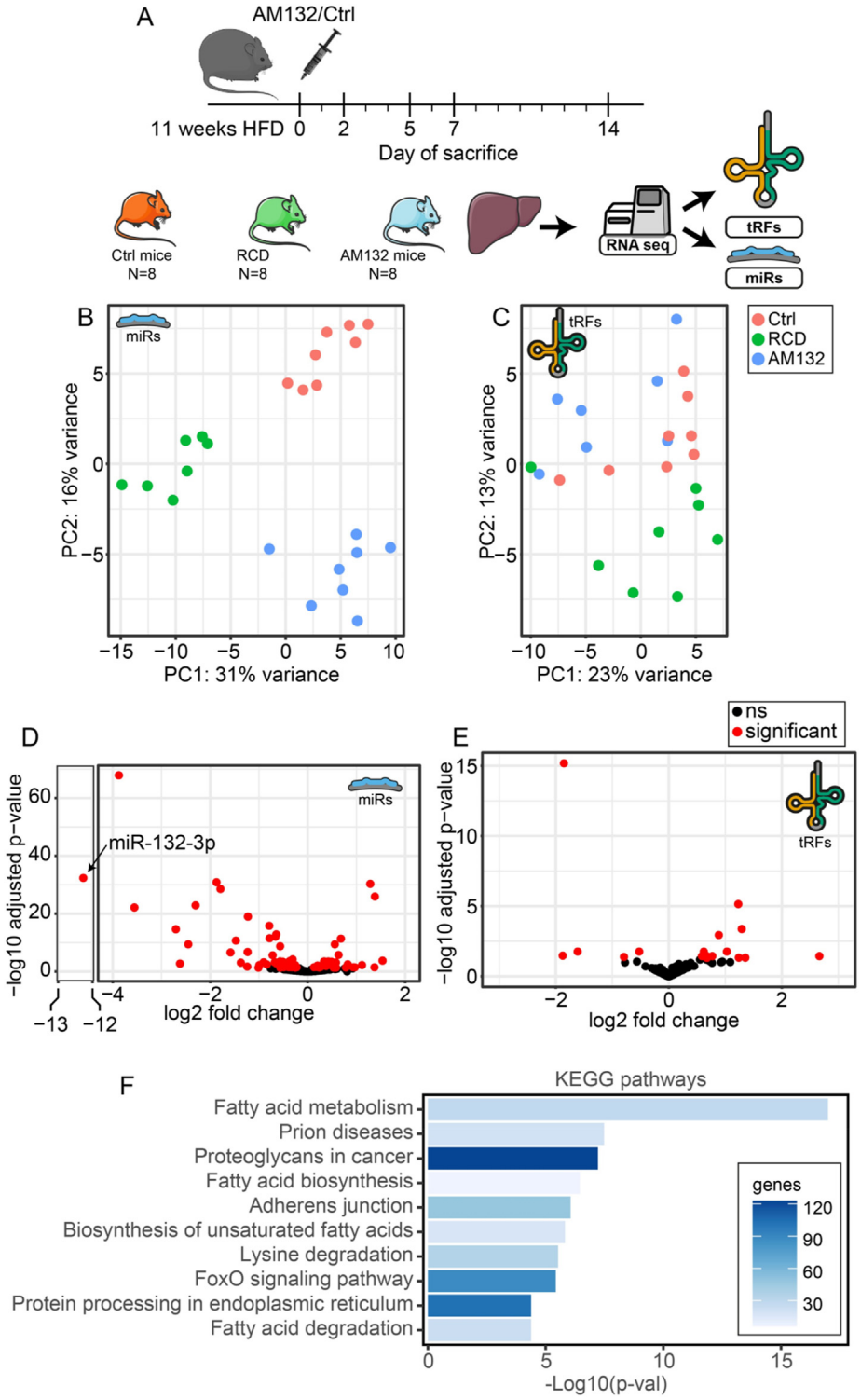

Figure 1: AM132-reversal of the fatty liver phenotype in DIO mice induced altered miR and tRF profiles. **A.** Experimental design: DIO mice injected with AM132 or AM608 as control (Ctrl) were sacrificed on day 7, with age-matched RCD mice (n = 8 per group). Liver samples were collected and small RNA-seq was performed to profile miRs and tRFs. **B.** PCA showing clustering of DE miRs according to treatment. **C.** PCA of DE tRFs also shows clustering according to treatment. **D.** Volcano plot of DE miRs in AM132-treated DIO mice vs control revealed larger fold changes in decreased vs increased miRs. **E.** Volcano plot of DE tRFs in these samples showed a mild increase in elevated tRFs. **F.** KEGG pathway analysis of the of the DE miR targets pointed to enrichment in fatty acid metabolism pathways.

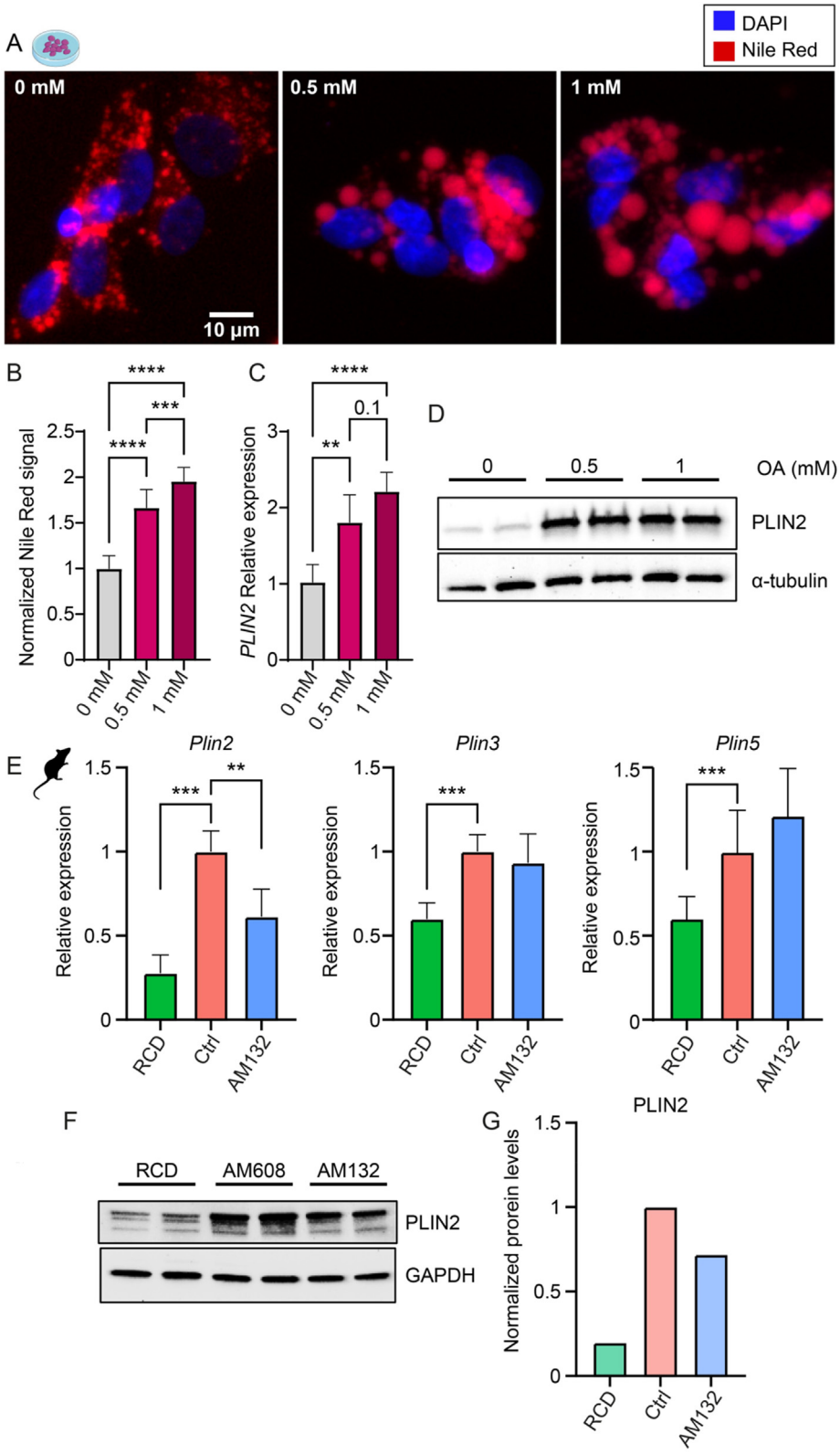

Figure 2: PLIN2 reflects lipid levels in human Hep G2 cells and DIO mice. **A.** Hep G2 cells exposed to 0, 0.5, or 1 mM OA for 48 h were fixed and stained with Nile Red (red) and DAPI (blue), and show increasing Nile Red accumulation that reflects increasing triglyceride content. **B.** Quantification of Nile Red signals in independent experiments by spectrophotometry, n = 3 experiments, multiple wells per experiment. Total Nile Red signal was normalized to total DAPI signal, per each well. **C.** RT-qPCR quantification of PLIN2 mRNA levels normalized to ribosomal protein RPL19 show OA-induced and dose-dependent enhancement of LD content. **D.** PLIN2 protein levels increase as well under OA treatment. **E.** AM132 treatment reduced Plin2 (but not Plin3 or Plin5) mRNA levels compared to Ctrl mice; quantification by RT-qPCR, normalization to b-actin (n = 5–8 per group). **F.** PLIN2 protein levels increase in DIO compared to RCD mice, but decrease under AM132 treatment (n = 2 per group). **G.** Quantification of PLIN2 immunoblot shown in panel F. In panels B, C, E, average ± SD, one-way ANOVA with Tukey's correction for multiple comparisons, *p < 0.05, **p < 0.01, ***p < 0.001, ****p < 0.0001.

reduced Plin2 levels due to selective regulation by DE miRs. To distinguish between these options, we focused on the top 10 miRs that were most DE between AM132-treated and Ctrl mice. Among those, miR-194-5p, which was elevated in the AM132-treated mice (Figure 1D, Supp. Table 1) was of special interest, as the TargetScan target prediction tool [38] identified it as targeting both human and mouse *PLIN2/Plin2* (Figure 3A). Correspondingly, miR-194-5p levels as determined by RT-qPCR were lower in the DIO (NAFLD-afflicted) Ctrl compared to AM132-treated mice (Figure 3B). In OA-exposed steatotic Hep G2 cells, the levels of miR-194-5p were also reduced, by ~10%

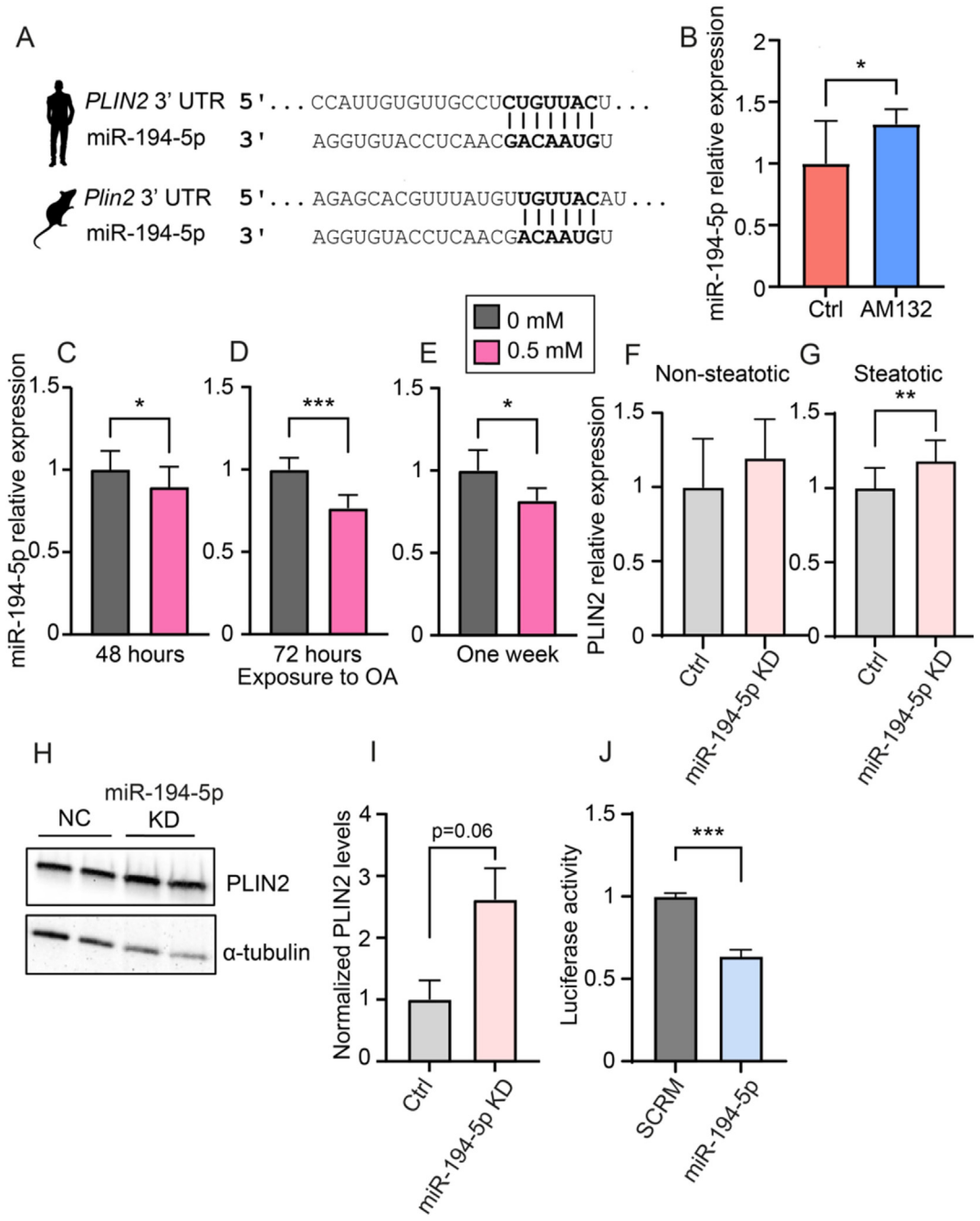

Figure 3: NAFLD-related miR-194-5p decline promotes PLIN2-mediated steatosis. **A.** The predicted complementary binding sites of miR-194-5p in human and murine PLIN2 mRNAs (upper and lower sections). **B.** RT-qPCR validation of RNA-seq presents elevated miR-194-5p levels in AM132 compared to control mice (n = 8 per group, RNA-seq in Figure 1D). **C.** miR-194-5p levels decline in steatotic Hep G2 cells following 48 h exposure to OA. **D.** miR-194-5p levels following 72 h of OA exposure. **E.** miR-194-5p levels following 1 week of OA exposure. Levels were determined by RT-qPCR and normalized to SNORD47, 2–3 experiments in each column. **F.** PLIN2 mRNA levels following miR-194-5p KD in non-steatotic cells show a statistically insignificant increase ($p = 0.13$). **G.** Significantly elevated PLIN2 mRNA levels following KD in steatotic Hep G2 cells. In panels F–G PLIN2 was measured by RT-qPCR and normalized to RPL19, 3 experiments each. **H.** PLIN2 protein increases following miR-194-5p KD in steatotic Hep G2 cells. **I.** Blot quantification of panel H, normalized to alpha-tubulin. **J.** Luciferase activity in HEK293T cells co-transfected with plasmids expressing human *PLIN2* 3′UTR and miR-194-5p or scrambled sequence. In panels B–G, I, J, average ± SD, Student's t-test, *$p < 0.05$, **$p < 0.01$, ***$p < 0.001$.

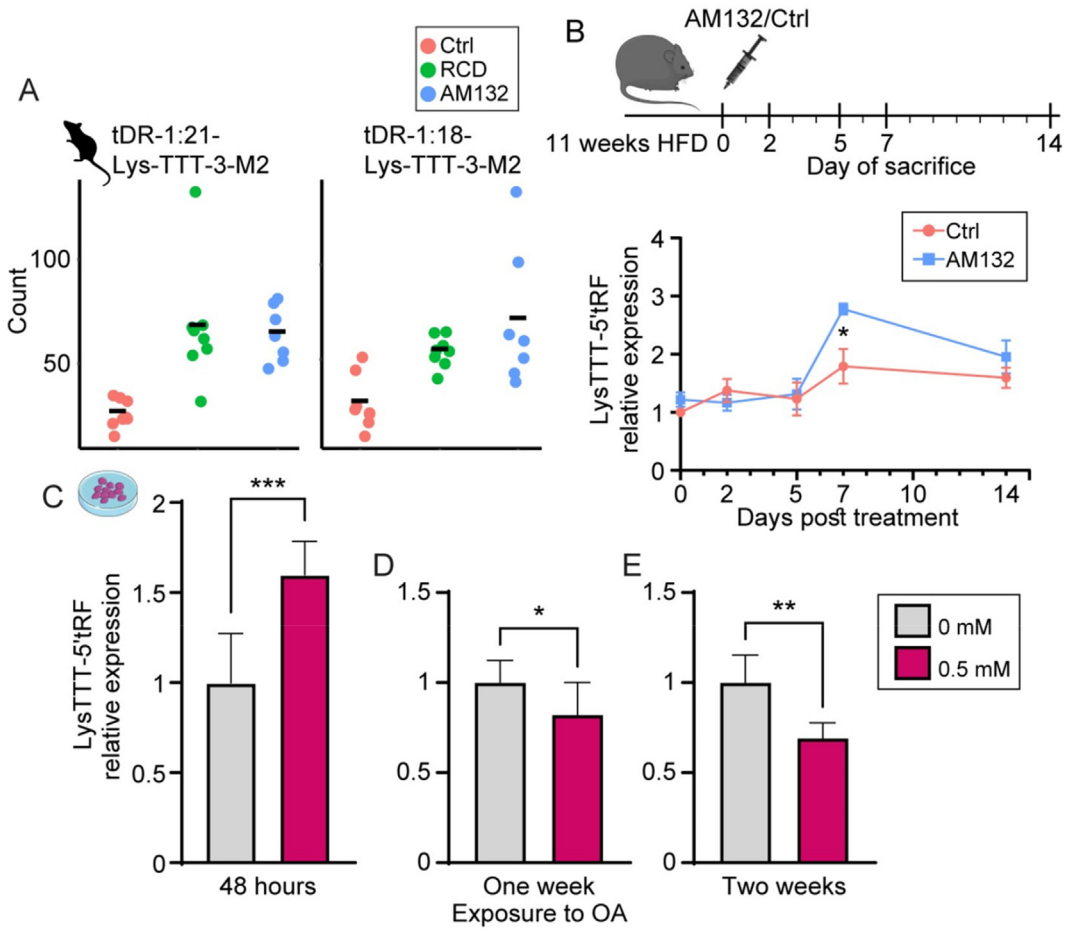

Figure 4: LysTTT-tRFs show NAFLD-related decline in vivo and in-vitro. **A.** The levels of two LysTTT-5′tRFs (tDR-1:21-Lys-TTT-3-M2 and tDR-1:18-Lys-TTT-3-M2) are reduced in NAFLD-afflicted Ctrl mice but restored to lean RCD mice levels under AM132 treatment. **B.** Experimental design (identical to Figure 1), with liver samples of AM132-treated and Ctrl mice collected at 0, 2, 5, 7 and 14 days after AM132 treatment (n = 4 per group). LysTTT-5′tRFs showed highest levels at day 7 after AM132 treatment ($p = 0.019$), when steatosis was lowest. **C.** LysTTT-5′tRF levels increase following acute 48 h exposure of Hep G2 cells to OA. **D**—**E.** LysTTT-5′tRF levels decrease following OA exposure for one and two weeks. Levels of tRF were determined by RT-qPCR after size selection and normalized to miR-145-5p and miR-15a-5p, average ± SD, Student's t-test, $^{*}p < 0.05$, $^{**}p < 0.01$, $^{***}p < 0.001$.

following 48 h of exposure to OA, and by ∼20% following longer exposure (Figure 3C—E). To further test PLIN2 targeting by miR-194-5p we performed knockdown (KD) of miR-194-5p in Hep G2 cells using antisense oligonucleotide (ASO) (Supp. Figure 2A). RT-qPCR of miR-194-5p confirmed full knockdown in both non-steatotic and steatotic Hep G2 cells (Supp. Figure 2B, C). Correspondingly, PLIN2 mRNA levels were elevated by ∼20% in both non-steatotic and steatotic cells (Figure 3F, G). This increase was significant in the steatotic cells (Figure 3G) and was reflected in protein levels, which were increased 2.5-fold (Figure 3H, I). In the non-steatotic cells this increase did not reach statistical significance, possibly due to the markedly lower PLIN2 levels in these cells, as demonstrated both at the mRNA and protein levels (Figure 2C, D), thus leading to a reduced impact of the KD.

To challenge direct PLIN2 regulation by miR-194-5p we co-transfected HEK293T cells with two plasmids, one expressing the 3′UTR of human *PLIN2* and the second expressing miR-194-5p or a scrambled control sequence (see Materials and Methods). We then performed a dual luciferase reporter assay and determined that transfection with miR-194-5p vs control reduced luciferase activity by ∼40% (Figure 3J), therefore confirming *PLIN2* as a novel target of miR-194-5p.

2.4. The anti-steatotic AM132 treatment elevates LysTTT-5′tRFs

To explore tRF involvement in NAFLD pathogenesis, we sought liver DE tRFs in the DIO mice which, following AM132 treatment, exhibit restored RCD levels (Figure 1E, Supp. Table 3) [25]. Among the top 10 DE tRFs, we focused on two sequence-sharing tRFs originated from LysTTT-tRNA; tDR-1:18-Lys-TTT-3-M2 and tDR-1:21-Lys-TTT-3-M2 (hereafter LysTTT-5′tRFs). These fulfilled the criteria of low levels in DIO Ctrl mice and elevation upon AM132 treatment to the levels observed in RCD mice (Figure 4A). To gain more insight into the expression kinetics of the LysTTT-5′tRFs in NAFLD, we further quantified their levels in liver samples of AM132 and Ctrl mice at 0, 2, 5, 7 and 14 days post-treatment (Figure 4B upper panel). This was done by performing electrophoretic size selection prior to RT-qPCR, to extract fragments smaller than 50 bases and exclude the amplification of intact tRNAs (see Materials and Methods and Supp. Table 5). AM132-treated mice presented progressively reduced liver steatosis, which reached its lowest level at day 7 post-treatment [25]. Interestingly, LysTTT-5′tRFs showed parallel, albeit inverse kinetics, with elevation initiating on day 5 post-treatment, reaching peak levels at day 7, and decreasing by day 14 post-treatment (Figure 4B lower panel). These

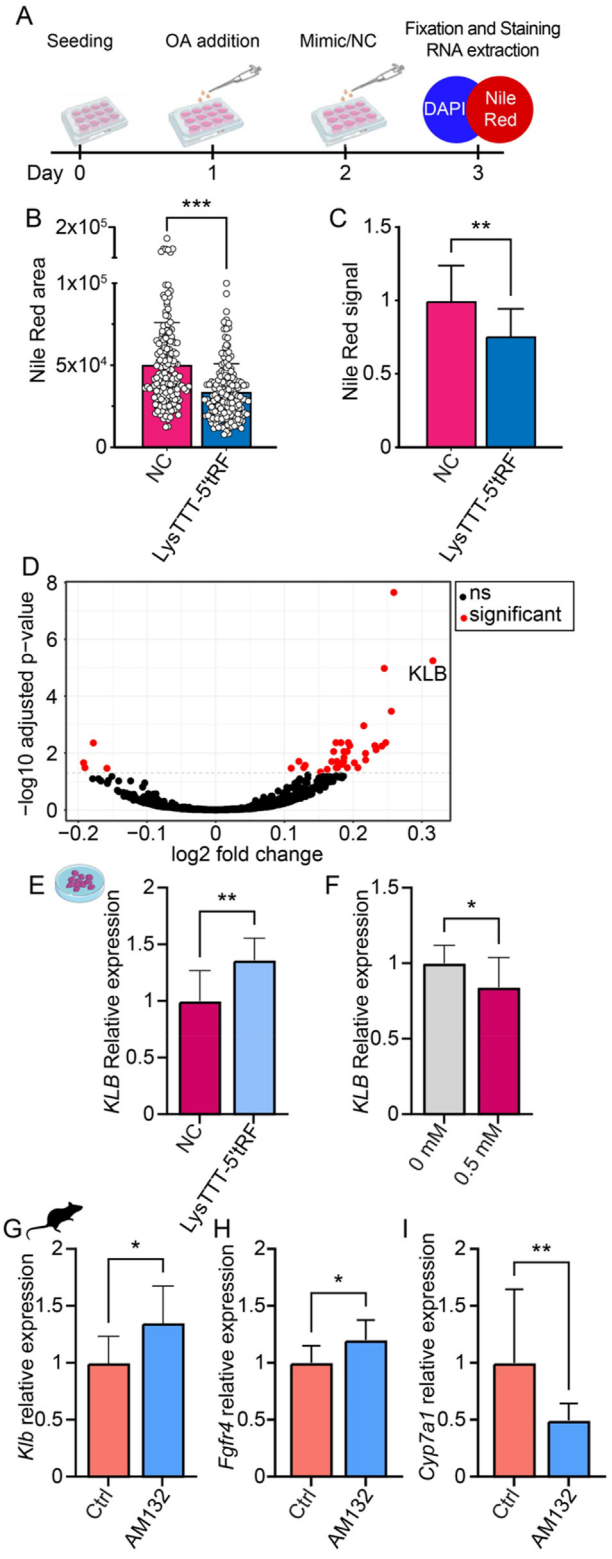

Figure 5: LysTTT-5′tRF suppresses steatosis in Hep G2 cells. A. Experimental design: 24 h after seeding, cells were exposed to 0.5 mM OA for 24 h, then transfected with 100 nM of a LysTTT-5′tRF mimic for 24 h. At 48 h after OA (24 h after mimic treatment) cells were fixed, stained and imaged or harvested for RNA extraction. **B.** Triglyceride levels were determined in >150 confocal microscope images from multiple wells in three independent experiments, expressed as area of Nile Red signal normalized to the number of nuclei per image. A 33% reduction in lipid content following LysTTT-5′tRF mimic treatment was observed. **C.** Triglyceride levels determined in 3 independent experiments by spectrophotometry, expressed as total Nile Red signal normalized to total DAPI signal per well. Note the 25% reduction in lipid content following LysTTT-5′tRF mimic treatment. **D.** RNA-seq of steatotic Hep G2 cells treated with LysTTT-5′tRF mimic compared to control, with KLB presenting the most profound fold change in treated cells (log2FoldChange = 0.3, p = 5.69E-06). **E.** RT-qPCR validation of the sequencing results showing that KLB mRNA levels were restored in steatotic cells following treatment with a LysTTT-5′tRF mimic. **F.** KLB mRNA levels show a decline in steatotic compared to non-steatotic Hep G2 cells. **G.** RT-qPCR quantification of Klb mRNA levels showing elevation in mice following AM132 treatment compared to Ctrl mice. **H.** RT-qPCR quantification of Fgfr4 mRNA levels likewise showing elevation following AM132 treatment. **I.** RT-qPCR quantification of Cyp7a1 showing reduced mRNA levels following AM132 treatment. In panels E, F, quantification by RT-qPCR, normalized to RPL19 (n = 3 experiments). In panels G–I, quantification by RT-qPCR, normalized to b-actin (n = 7–8 mice per group). In all panels except A and D, average ± SD, Student's t-test, *p < 0.05, **p < 0.01, ***p < 0.001.

parallel timelines suggested a functional involvement of the tRFs in reversing the fatty liver phenotype.

To gain more insight into the function of LysTTT-5′tRFs we first tested their levels in our Hep G2 steatosis model. Contrasting the decrease observed in the DIO Ctrl relative to the AM132 mice, 48 h of OA exposure led to elevation of LysTTT-5′tRF levels by 50% (Figure 4C). However, since NAFLD is a chronic liver disease in which patients are subjected to constant hepatic lipid load, often for years, we suspected that the acute 48 h OA exposure in cell culture was insufficient to recapitulate the long-term aspects of NAFLD. To more closely mimic the chronic lipid overload we exposed Hep G2 cells to OA for one and two weeks. Under those conditions LysTTT-5′tRFs levels were decreased by ~20% and ~30% (Figure 3D, E), compatible with their reduction in the NAFLD-afflicted mice.

2.5. LysTTT-5′tRF mimic suppresses lipid droplet accumulation and elevates β-Klotho (KLB) levels

To pursue causal effects of LysTTT-5′tRFs on triglyceride accumulation we treated OA-exposed steatotic Hep G2 cells with a chemically protected RNA oligonucleotide mimic of LysTTT-5′tRF or a negative control (NC) RNA oligonucleotide (Figure 5A, Supp. materials and methods). Following staining with Nile Red and DAPI we acquired confocal microscopy images of these cells (n = ~150, multiple wells from three independent experiments) and determined lipid droplet levels by using our computational tool (see Supp. materials and methods and Supp File 1 for details) to quantify the total area of Nile Red signal and normalize it to the number of DAPI-stained nuclei. Within 24 h, mimic-treated cells showed a 33% reduction in Nile Red staining area compared to NC-treated cells (Figure 5B). To re-challenge this observation we quantified lipid droplets in three independent experiments by spectrophotometric measurement of Nile Red and DAPI staining (reflecting cell number, see Supp. materials and methods), which revealed that cells treated with the LysTTT-5′tRF mimic showed ~25% lower signal intensity, substantiating the expedited 24 h-reduction in triglyceride levels (Figure 5C).

To further seek downstream changes in response to LysTTT-5′tRF enrichment we performed long RNA-seq of steatotic Hep G2 cells treated with LysTTT-5′tRF mimic or NC oligonucleotides. This analysis revealed 32 DE transcripts, 28 of which were upregulated following mimic compared to NC treatment (Supp. Table 4). Importantly, the transcript with the largest fold change upon LysTTT-5′tRFs mimic treatment was *KLB*, elevated by ~25% (Figure 5D). These results were also verified by qPCR quantification in independent experiments that showed *KLB* levels elevated by ~35% (Figure 5E). KLB, an essential co-factor of FGFR, is known for its protective role in NAFLD [18]. To challenge its involvement in regulating triglyceride

accumulation in our cell culture system, we measured *KLB* levels following OA exposure. Notably, *KLB* levels were reduced in the steatotic Hep G2 cells (Figure 5F). Taken together, these results show the beneficial effect of the LysTTT-5′tRF mimic that is able to restore *KLB* levels following their reduction under steatosis. Compatible with our findings in the Hep G2 model, DIO mice as well revealed elevated levels of hepatic *Klb* mRNA levels following steatosis-alleviating AM132 treatment (Figure 5G). Upregulated *Klb* levels could potentially suggest increased FGFR4-KLB mediated signaling; to challenge this prediction as well, we next quantified the levels of expressed Fgfr4 and found those levels to be elevated as well following AM132 treatment, at a similar extent to the *Klb* increases (Figure 5H). Downstream intracellular responses to FGFR4-KLB signaling include the inhibition of bile acid synthesis by downregulation of cholesterol 7a-hydroxylase (CYP7A1). Correspondingly, the AM-132-treated mice presented *Cyp7a1* levels reduced by ∼50% (Figure 5I). Together, these findings suggest that increased levels of LysTTT-5′tRF reduce triglyceride accumulation while elevating KLB to activate FGFR4-KLB mediated signaling.

2.6. Danazol and Latanoprost reduce steatosis and elevate LysTTT-5′tRF and miR-194-5p

To characterize potential pathways/targets which involve LysTTT-5′tRF and miR-194-5p and reduce steatosis, we next performed a screening assay of 1600 drugs from a drug repurposing compound library composed of phase-I-approved therapeutics (Figure 6A and Materials and Methods). Notably, 15 of the 1600 tested drugs decreased lipid accumulation by over 40% within 24 h (Figure 6B). Intriguingly, these drugs include anti-infection drugs (Fosamprenavir, Maribavir, Bephenium and Pentoxifylline), anti-inflammation drugs (Diphenylpyraline and Naproxen), and others (Figure 6C). Having identified those compounds which reduce triglyceride levels, we sought corresponding changes in LysTTT-5′tRF and miR-194-5p levels. This search revealed that treatment with Danazol (pink) elevated the levels of LysTTT-5′tRF, whereas treatment with Latanoprost (green) elevated miR-194-5p (Supp. Figure 3A, B). Danazol is a synthetic steroid that suppresses gonadotrophin production and possesses some weak androgenic effects, and Latanoprost is a prostaglandin F2α analog that is used to treat elevated intraocular pressure. Notably, the remaining drugs showed no effect on the two NAFLD-related sncRNAs. That only two drugs altered the levels of LysTTT-5′tRF and miR-194-5p emphasized the involvement of multiple pathways and various factors in eliciting steatosis, ultimately presenting the complexity of NAFLD pathophysiology and its diverse patterns of cell type specificities.

3. DISCUSSION

Challenging the working hypothesis that NAFLD's development and progression may involve active role(s) of sncRNAs, we used small RNA-seq to profile the hepatic levels of miRs and tRFs in healthy and fattened mice with or without the steatosis-alleviating AM132 treatment. This identified joint declines of LysTTT-5′tRFs and miR-194-5p in NAFLD-afflicted mice and in steatotic HepG2 cells, and noted inverse yet transient rescue of their levels following AM132 treatment. Taken together, our findings predicted potential roles for these sncRNAs in human NAFLD.

Unlike blood cells from ischemic stroke patients, which show a 'changing of the guard' phenomenon in which cholinergic-targeting miRs are replaced by tRFs [39], or the sex-specific and disease-related loss of cholinergic-targeted tRFs in the brains of women living with Alzheimer's disease [40], our current study revealed hepatic 'in tandem' decline of LysTTT-5′tRFs and miR-194-5p, which may jointly contribute to the steatosis process through complementary impacts on distinct pathways. Supporting human relevance, miR-194-5p decline also occurred in human-originated Hep G2 cells following a short 48 h exposure to OA (∼10%), with further reduction after 72 h and one week exposure to OA (∼20%). In contrast, LysTTT-5′tRFs levels were first elevated following acute 48 h of exposure to OA but were reduced following longer exposures of one and two weeks to OA. Thus, LysTTT-5′tRFs could provide an 'emergency' control, with miR-194-5p providing a longer-term impact. The 'emergency' response pattern of LysTTT-5′tRFs is further compatible with the fact that tRFs would be more readily available to deal with acute insults since no transcription is required to elevate tRF levels, which are processed from already existing tRNAs in the cytoplasm and are unavoidably present in all cells. In contrast, miRs would first have to be transcribed in the nucleus and then exported to the cytoplasm [19,28]. The initial elevation in LysTTT-5′tRF levels following short exposure to OA may potentially reflect a cellular attempt to cope with the stress condition under lipid overload, which may lead to enhanced tRNA cleavage and LysTTT-5′tRF production. However, after prolonged exposure to OA, the hepatocyte tRNA reservoir may be depleted, ultimately resulting in decreased levels of LysTTT-5′tRFs and weaker protection from LD accumulation.

Of particular interest, each of the identified small RNAs targets distinct albeit metabolically relevant pathways. Specifically, we uncovered a novel anti-steatotic role of miR-194-5p by identifying the main hepatic LD-coating protein PLIN2 as its direct target. This finding adds to others' reports of miR-194-5p control over hepatic stellate cell activation which is implicated in the development of liver fibrosis. Moreover, it relates to findings of miR-194-5p downregulation in fibrotic liver [41,42] and in NASH and cirrhosis patients compared to controls, and to its being marked as a potential diagnostic marker for NAFLD [43]. Furthermore, a NAFLD-protective role of miR-194-5p was proposed based on its elevated levels in DIO mice treated with green tea over 12 weeks and on its capacity to decrease the uptake and accumulation of lipids via the Hmgcr and Apoa5 transcripts influencing triglyceride metabolism and fatty acid catabolism [44]. Adding to its anti-fibrotic effects, our finding of PLIN2 as a miR-194-5p target indicates that the loss of miR-194-5p in NAFLD and fibrosis may further promote steatosis and contribute to NAFLD progression.

Others have also proposed tRF involvement in NAFLD pathophysiology; tRF-3001b may promote NAFLD progression by inhibiting autophagy through targeting the Prkaa1 gene [45], and the levels of three plasma tRFs (tRF-Val-CAC-005, tiRNA-His-GTG-001, and tRF-Ala-CGC-006) are elevated in NAFLD patients and mouse models, reflecting the degree of liver fibrosis [46]. In comparison, we found that LysTTT-5′tRFs protect from NAFLD by reducing triglyceride accumulation in steatotic Hep G2 cells, and that this involved restoration of *KLB* levels. Notably, KLB emerged as a promising target for treating NAFLD based on its role as an important mediator of FGF19 signaling [18]. The expression of FGF19 is induced in enterocytes by liver-derived BA binding to the farnesoid X receptor. FGF19 is then secreted to the liver where it binds the FGFR4-KLB complex, and induces downstream intracellular responses which include the inhibition of BA synthesis by downregulation of cholesterol 7a-hydroxylase (CYP7A1) [16,47–49]. Importantly, impaired BA synthesis and homeostasis are closely implicated in NAFLD [14,15]. Indeed, mice treated with AM132 showed increased Klb and Fgfr4 levels and decreased Cyp7a1 levels, indicating higher FGF19 signaling activity. Moreover, the KLB rs17618244 variant increases the risk of ballooning and lobular

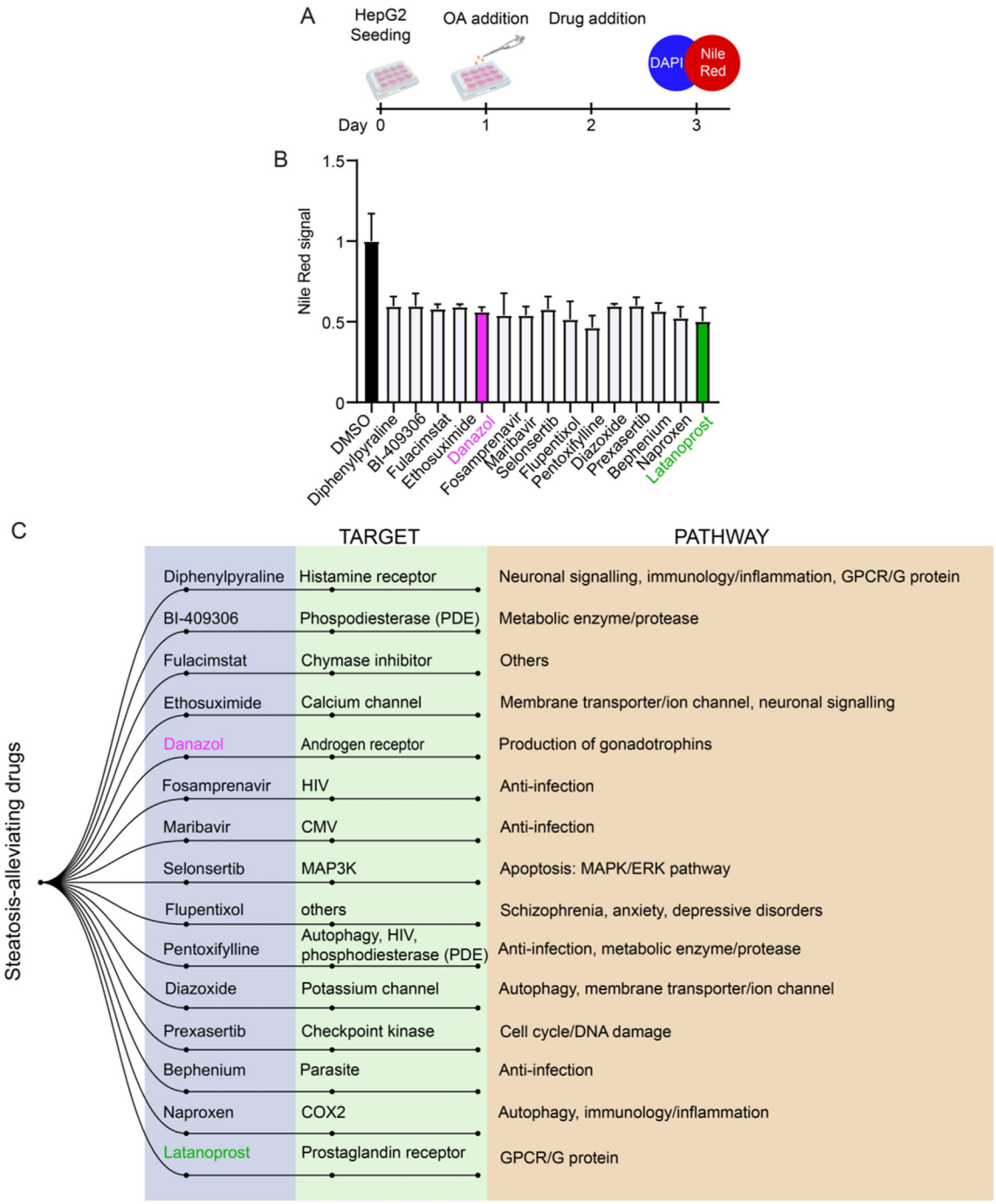

Figure 6: Novel steatosis-alleviating drugs reveal the multilayered complexity of NAFLD. **A.** Experimental design: At 24 h post-seeding cells were exposed to 0.5 mM OA for 24 h, transfected with 5 μM of each of the tested drugs for 24 h, then fixed for staining. Triglyceride content was quantified by spectrophotometry, with total Nile Red signal per well normalized to total DAPI signal per well. **B.** 15 out of 1600 candidate drugs targeting diverse pathways decreased lipid accumulation in steatotic Hep G2 cells by over 40% within 24 h. **C.** Scheme of the 15 candidate steatosis-alleviating drugs (purple), their known targets and properties (green), and pathways through which they act (brown). In panel B average ± SD, Student's t-test, $^{**}p < 0.01$.

inflammation in children with NAFLD, and carriers of this single nucleotide polymorphism present lower levels of hepatic and plasma KLB. Furthermore, KLB downregulation in HepG2 and Huh7 cells induced steatosis and upregulation of pro-inflammatory genes [50], and Klb-deficient mice present steatosis and increased levels of pro-inflammatory cytokines [51].

Whether LysTTT-5′tRF elevation directly regulates KLB mRNA levels requires further identifying of possible mechanism(s) leading to this effect. Several tRFs are known to affect mRNA stability by interacting with RNA-binding proteins; in breast cancer cells, certain tRFs derived from Glu-, Asp-, Gly-,Tyr-tRNAs suppress the stability of oncogenic transcripts by interacting with the YBX1 protein and displacing it from

the 3′UTR [52]. Also, 5′-tRF derived from Cys-tRNA binds to nucleolin and induces its oligomerization, which in turn enhances nucleolin-bound mRNAs' stability [53]. However, whether that is the case for LysTTT-5′tRFs and elevated *KLB* levels requires future research.
Intriguingly, both Danazol and Latanoprost, the two approved drugs exerting response of LysTTT-5′tRFs and miR-194-5p in steatotic Hep G2 cells, target androgen receptors (Danazol) and FP prostanoid receptors (Latanoprost). However, to the best of our knowledge, neither of those was tested for treating NAFLD. In conclusion, we identified two sncRNAs, LysTTT-5′tRF and miR-194-5p, which jointly yet distinctly regulate lipid accumulation in hepatocytes via different mechanisms, and indicate multiple pathways for sncRNAs involvement in NAFLD development and progression.

4. MATERIALS AND METHODS

4.1. Mice

Animal studies were approved by the ethics committees of The Hebrew University of Jerusalem (approvals 14-14135-3 and NS-16-148663-3). C57bl/6J mice were fed a regular chow diet (RCD) or a high fat diet (Harlan Teklad, Madison, Wisconsin, USA) for 11 weeks to reach diet-induced obesity. Injected oligonucleotides were modified by locked nucleic acid protection and complementary to mature miR-132 (AM132, 16-mer) or to mature primate-specific miR-608 (AM608, 15-mer, as a control with no predicted complementary sequences in mice) (LNA, Exiqon, Qiagen). DIO mice were injected intravenously with 3.3 mg/kg oligonucleotide for three consecutive days and were sacrificed 0, 2, 5, 7, and 14 days post-treatment. Liver and hypothalamus samples were collected, snap frozen in liquid nitrogen, and stored at −80 °C. Age matched RCD mice were sacrificed and livers collected as above [25].

4.2. Cell culture and tRF mimic experiments

Human hepatocellular carcinoma Hep G2 cells (HEPG2, ATTC HB-8065™) were used in all experiments and were grown under standard conditions (Supp. materials and methods). Cells were treated with oleic acid (OA)-rich medium (Supp. materials and methods) for 24 h and transfected with 100 nM LysTTT-5′tRF mimic or negative control oligonucleotide (IDT, Syntezza Bioscience, see Supp. materials and methods for sequences) using the HiPerFect transfection reagent (Qiagen, 301705). After incubation for an additional 24 h in the same OA-rich medium, cells were harvested for RNA and protein extraction or fixed for triglyceride quantification.

4.3. RNA extraction

RNA was extracted using the miRNeasy Mini Kit (Qiagen, 217004) according to the manufacturer's protocol, followed by determination of RNA concentration (NanoDrop 2000, Thermo Scientific), standard gel electrophoresis for quality assessment, and RIN determination (Bioanalyzer 6000, Agilent).

4.4. RT-qPCR

Synthesis of cDNA and RT-qPCR for mRNAs, miRs, and tRFs were done using Quantabio reagents and mouse or human-specific primers (see Supp. materials and methods for reagent details and Supp. Table 5 for primer sequences). The CFX384 Touch Real-Time PCR System (Bio-Rad) was used for quantification and the CFX Maestro software (Bio-Rad v4.1.2433.1219) for analysis. Data is presented as relative expression (ΔΔCt) normalized to housekeeping genes and plotted in GraphPad Prism 8.0 (GraphPad Prism Software).

4.5. Immunoblotting

Cells were seeded in 12-well plates and incubated in 0, 0.5, or 1 mM OA-rich medium for 24 h prior to transfection with a tRF mimic for 24 h. Cells were then washed and lysed in RIPA buffer, protein concentrations were determined, and 5 μg/sample were loaded and separated by 4—15% gradient polyacrylamide gels and transferred to nitrocellulose membranes. Proteins were detected with antibodies against PLIN2 (Proteintech, 15294-1-AP), KLB (Abcam, ab106794) and Alpha-Tubulin (Merck, T5168), HRP-conjugated secondary antibodies (Jackson, 111-035-144 and 115-035-062), then ECL (Cell Signaling Technologies, 12757 or Thermo Fisher Scientific, 34580) using the myECL™ Imager and its software (Thermo Fisher Scientific) (see Supp. materials and methods for details).

4.6. Triglyceride quantification

Cells were washed, fixed with 4% PFA, permeabilized, and stained with DAPI (1 μg/mL, Santa Cruz Biotechnology, sc-3598) followed by Nile Red (300 nM, Thermo Fisher Scientific, N1142). A Tecan Spark™ 10M plate reader was used for spectrophotometric quantification, with triglyceride content per well expressed as total Nile Red signal normalized to total DAPI signal. Quantification was also carried out by ImageJ analysis [54] of over 150 confocal microscope images (FLUOVIEW FV10i, Olympus) from three independent experiments, with triglyceride content per image expressed as total area of Nile Red signal normalized to number of nuclei (See Supp. materials and methods for method details and analysis parameters). The code is publicly available, suitable for LD quantification and easy to adjust and repurpose.

4.7. miR-194-5p knockdown

Cells were seeded in 12-well plates (150,000 cells/well) and transfected 24 h later with 100 nM antisense oligonucleotide targeting miR-194-5p or miR-608 as control (miR-608 is not expressed in Hep G2 cells) (Exiqon, Qiagen) using Lipofectamine™ 3000 Transfection Reagent (Thermo Fisher Scientific, L3000008). 48 h later cells were harvested. For RNA extraction, cells were collected in QIAzol with RNA extraction as above. For protein extraction, cells were washed in PBS and lysed in 140 μl of RIPA buffer (see Supp. materials and methods) containing Protease Inhibitor Cocktail and Phosphatase Inhibitor Cocktail (1:100; Cell Signaling Technology, 5871 and 5870). Cells were incubated for 20 min on ice, collected and centrifuged twice (15 min, 20,000 g, 4 °C). Supernatants were transferred to fresh tubes and protein concentration was determined by Lowry assay (Bio-Rad, 5000113).

4.8. Dual luciferase assay

HEK293T cells were seeded in 24-well plates, and 24 h later co-transfected with 500 ng psiCHECK™-2 Vector (Promega) containing the 3′UTR of the human PLIN2 gene downstream to the Renilla luciferase gene, and with 500 ng plasmid expressing either miR-194-5p or a scrambled sequence as control (MR01 backbone, GeneCopoeia). 24 h later, cells were lysed and assayed using the Dual-Luciferase® Reporter Assay System (Promega, E1910) as per the manufacturer's instructions, using a Tecan Spark™ 10M plate reader. Results are expressed as ratio of Renilla to firefly luciferase activity for miR-194-5p normalized to scrambled.

4.9. Drug screening assay

1600 drugs of a 2800-compound library (HY-L035, MedChem Express, NJ, USA) were screened for identification of novel potential therapeutic

targets to alleviate steatosis. Cells were seeded in 96-well plates (20,000 cells/well) and 24 h later incubated with 0.5 Mm OA. 24 h later the drugs were introduced at a final concentration of 5 μM with 2.5% DMSO as control. After 24 h incubation, medium was removed and cells were washed and stained for DAPI and Nile Red. Triglyceride quantification was performed using a plate reader as describe above and in Supp. materials and methods.

4.10. Small RNA sequencing and analysis

Murine tissues: RNA was extracted as described above from liver (n = 8 per group) and hypothalamus (n = 12–16 per group) samples of obese mice injected with AM132 or AM608 and lean RCD mice. RIN was determined to be above 8.4 for all samples. Libraries were constructed from 300 ng (liver) or 200 ng (hypothalamus) total RNA (NEBNext Multiplex Small RNA library prep set for Illumina, New England Biolabs, NEB-E7560S) and the small RNA fraction was sequenced on the NextSeq 500 System (Illumina) at the Center for Genomic Technologies Facility, the Hebrew University of Jerusalem.

Hep G2 cells: RNA was extracted from steatotic cells treated with LysTTT-5′tRF mimic or NC (two replicates per treatment) as described above and RIN determined to be above 9.5 for all samples. Libraries were constructed from 500 ng total RNA using KAPA Stranded mRNA-Seq Kit (KAPA Biosystems, Wilmington, USA) and sequenced on NextSeq 2000 (Illumina).

Analysis: FastQC (http://www.bioinformatics.babraham.ac.uk/projects/fastqc/) was used for quality control and reads were further trimmed and filtered using Flexbar (version 0.11.9 [55]). Sequences were aligned using miRExpress 2.1.4 [56] (liver) or miRDeep2 [57] (hypothalamus) to miRBase version 21 for microRNAs or using MINTmap 1.0 for conserved tRFs in mouse and human [58]. For the long RNA sequencing exclusion of potential rRNA sequences was done using Bowtie2 [59] and performing the alignment to the reference genome (GRCh38.p14, release 109) using STAR aligner [60]. The transcripts were subsequently quantified using HTSeq [61].

Differential expression analysis was performed in R version 4.1.3 using DESeq2 [62]. MiRs, tRFs and long transcripts were considered DE if they presented adjusted p-value of <0.05. Shrunken log2fold changes were calculated with the "apeglm" algorithm [63] in small RNA expression datasets and "normal" in the mimic experiment. Outlier samples in liver were excluded based on PCA plots. Determination of outliers was conducted with sample clustering by PCA. For liver samples, sample AM132.8 was excluded for DE tests in the tRF analysis, and sample RCD.3 was excluded from the miR analysis.

4.11. tRF size selection and qPCR

To validate sequencing results we isolated tRFs from total RNA samples, while excluding whole tRNA molecules, as follows: 1 ug total RNA per sample were separated by PAGE and bands containing RNAs less than 50 nucleotides long were excised from the gel based on two size markers. RNA was eluted from the gel, ethanol-precipitated, and recovered in ddw. cDNA was synthesized from 500 pg/sample and tRF levels were quantified by qPCR as described above. (See Supp. materials and methods for detailed protocol).

FUNDING AND ACKNOWLEDGMENTS

The research leading to these results received funding by the Israel Science Foundation, ISF (1016/18; to H. Soreq), by a joint research support to H. Soreq and I. Paldor from Hebrew University and the Shaarei Zedek Medical center and by the Ken Stein foundation. YT's and NM's fellowships were supported by the US friends of the Hebrew University of Jerusalem and The Sephardic Foundation on Aging (New York). KW was a Shimon Peres post-doctoral Fellow at ELSC and SD is an Azrieli PhD fellow. Parts of the figures in this article were created with BioRender.com.

DECLARATION OF COMPETING INTEREST

The authors declare that they have no known competing financial interests or personal relationships that could have appeared to influence the work reported in this paper.

DATA AVAILABILITY

The original gene expression data (FASTQ files, metadata and tables of raw counts) from the DIO mice (liver and hypothalamus samples) and Hep G2 cells are available at the NCBI GEO database under the accession numbers GSE248319, GSE248321 and GSE248320. All other relevant datasets have been included as supplementary files to the manuscript and the original files and code are available upon request from corresponding author (hermona.soreq@mail.huji.ac.il).

APPENDIX A. SUPPLEMENTARY DATA

Supplementary data to this article can be found online at https://doi.org/10.1016/j.molmet.2023.101856.

REFERENCES

[1] Byrne CD, Targher G. NAFLD: a multisystem disease. J Hepatol 2015;62(1 Suppl.):S47–64.
[2] Olzmann JA, Carvalho P. Dynamics and functions of lipid droplets. Nat Rev Mol Cell Biol 2019;20(3):137–55.
[3] Cotter TG, Rinella M. Nonalcoholic fatty liver disease 2020: the state of the disease. Gastroenterology 2020;158(7):1851–64.
[4] Buzzetti E, Pinzani M, Tsochatzis EA. The multiple-hit pathogenesis of non-alcoholic fatty liver disease (NAFLD). Metabolism 2016;65(8):1038–48.
[5] Yki-Jarvinen H. Non-alcoholic fatty liver disease as a cause and a consequence of metabolic syndrome. Lancet Diabetes Endocrinol 2014;2(11):901–10.
[6] Scorletti E, Carr RM. A new perspective on NAFLD: focusing on lipid droplets. J Hepatol 2022;76(4):934–45.
[7] Itabe H, Yamaguchi T, Nimura S, Sasabe N. Perilipins: a diversity of intracellular lipid droplet proteins. Lipids Health Dis 2017;16(1):83.
[8] Orlicky DJ, Libby AE, Bales ES, McMahan RH, Monks J, La Rosa FG, et al. Perilipin-2 promotes obesity and progressive fatty liver disease in mice through mechanistically distinct hepatocyte and extra-hepatocyte actions. J Physiol 2019;597(6):1565–84.
[9] Chang BH, Li L, Paul A, Taniguchi S, Nannegari V, Heird WC, et al. Protection against fatty liver but normal adipogenesis in mice lacking adipose differentiation-related protein. Mol Cell Biol 2006;26(3):1063–76.
[10] McManaman JL, Bales ES, Orlicky DJ, Jackman M, MacLean PS, Cain S, et al. Perilipin-2-null mice are protected against diet-induced obesity, adipose inflammation, and fatty liver disease. J Lipid Res 2013;54(5):1346–59.
[11] Friedman SL, Neuschwander-Tetri BA, Rinella M, Sanyal AJ. Mechanisms of NAFLD development and therapeutic strategies. Nat Med 2018;24(7):908–22.
[12] Moschen AR, Kaser S, Tilg H. Non-alcoholic steatohepatitis: a microbiota-driven disease. Trends Endocrinol Metab 2013;24(11):537–45.
[13] Somm E, Henry H, Bruce SJ, Aeby S, Rosikiewicz M, Sykiotis GP, et al. beta-Klotho deficiency protects against obesity through a crosstalk between liver, microbiota, and brown adipose tissue. JCI Insight 2017;2(8).

[14] Arab JP, Karpen SJ, Dawson PA, Arrese M, Trauner M. Bile acids and nonalcoholic fatty liver disease: molecular insights and therapeutic perspectives. Hepatology 2017;65(1):350–62.
[15] Clifford BL, Sedgeman LR, Williams KJ, Morand P, Cheng A, Jarrett KE, et al. FXR activation protects against NAFLD via bile-acid-dependent reductions in lipid absorption. Cell Metab 2021;33(8):1671–1684 e4.
[16] Kurosu H, Kuro OM. The Klotho gene family as a regulator of endocrine fibroblast growth factors. Mol Cell Endocrinol 2009;299(1):72–8.
[17] Jahn D, Rau M, Hermanns HM. Geier A. Mechanisms of enterohepatic fibroblast growth factor 15/19 signaling in health and disease. Cytokine Growth Factor Rev 2015;26(6):625–35.
[18] Aaldijk AS, Verzijl CRC, Jonker JW, Struik D. Biological and pharmacological functions of the FGF19- and FGF21-coreceptor beta klotho. Front Endocrinol 2023;14:1150222.
[19] Gebert LFR, MacRae IJ. Regulation of microRNA function in animals. Nat Rev Mol Cell Biol 2019;20(1):21–37.
[20] Agbu P, Carthew RW. MicroRNA-mediated regulation of glucose and lipid metabolism. Nat Rev Mol Cell Biol 2021;22(6):425–38.
[21] Singh RP, Massachi I, Manickavel S, Singh S, Rao NP, Hasan S, et al. The role of miRNA in inflammation and autoimmunity. Autoimmun Rev 2013;12(12):1160–5.
[22] Banerjee J, Khanna S, Bhattacharya A. MicroRNA regulation of oxidative stress. Oxid Med Cell Longev 2017;2017:2872156.
[23] Su Q, Kumar V, Sud N, Mahato RI. MicroRNAs in the pathogenesis and treatment of progressive liver injury in NAFLD and liver fibrosis. Adv Drug Deliv Rev 2018;129:54–63.
[24] Gjorgjieva M, Sobolewski C, Dolicka D, De Sousa MC, Foti M. miRNAs and NAFLD: from pathophysiology to therapy. Gut 2019;68(11):2065–79.
[25] Hanin G, Yayon N, Tzur Y, Haviv R, Bennett ER, Udi S, et al. miRNA-132 induces hepatic steatosis and hyperlipidaemia by synergistic multitarget suppression. Gut 2018;67(6):1124–34.
[26] Maute RL, Schneider C, Sumazin P, Holmes A, Califano A, Basso K, et al. tRNA-derived microRNA modulates proliferation and the DNA damage response and is down-regulated in B cell lymphoma. Proc Natl Acad Sci U S A 2013;110(4):1404–9.
[27] Kuscu C, Kumar P, Kiran M, Su Z, Malik A, Dutta A. tRNA fragments (tRFs) guide Ago to regulate gene expression post-transcriptionally in a Dicer-independent manner. RNA 2018;24(8):1093–105.
[28] Kumar P, Kuscu C, Dutta A. Biogenesis and function of transfer RNA-related fragments (tRFs). Trends Biochem Sci 2016;41(8):679–89.
[29] Su Z, Wilson B, Kumar P, Dutta A. Noncanonical roles of tRNAs: tRNA fragments and beyond. Annu Rev Genet 2020;54:47–69.
[30] Zhu L, Ge J, Li T, Shen Y, Guo J. tRNA-derived fragments and tRNA halves: the new players in cancers. Cancer Lett 2019;452:31–7.
[31] Xie Y, Yao L, Yu X, Ruan Y, Li Z, Guo J. Action mechanisms and research methods of tRNA-derived small RNAs. Signal Transduct Target Ther 2020;5(1):109.
[32] Lobentanzer S, Hanin G, Klein J, Soreq H. Integrative transcriptomics reveals sexually dimorphic control of the cholinergic/neurokine interface in schizophrenia and bipolar disorder. Cell Rep 2019;29(3):764–777 e5.
[33] Long JK, Dai W, Zheng YW, Zhao SP. miR-122 promotes hepatic lipogenesis via inhibiting the LKB1/AMPK pathway by targeting Sirt1 in non-alcoholic fatty liver disease. Mol Med 2019;25(1):26.
[34] Vlachos IS, Kostoulas N, Vergoulis T, Georgakilas G, Reczko M, Maragkakis M, et al. DIANA miRPath v.2.0: investigating the combinatorial effect of microRNAs in pathways. Nucleic Acids Res 2012;(40(Web Server issue):W498–W504.).
[35] Zhang X, Ji X, Wang Q, Li JZ. New insight into inter-organ crosstalk contributing to the pathogenesis of non-alcoholic fatty liver disease (NAFLD). Protein Cell 2018;9(2):164–77.
[36] Adams LA, Feldstein A, Lindor KD, Angulo P. Nonalcoholic fatty liver disease among patients with hypothalamic and pituitary dysfunction. Hepatology 2004;39(4):909–14.
[37] Gomez-Lechon MJ, Donato MT, Martínez-Romero A, Jiménez N, Castell JV, O'Connor JE. A human hepatocellular in vitro model to investigate steatosis. Chem Biol Interact 2007;165(2):106–16.
[38] Agarwal V, Bell GW, Nam JW, Bartel DP. Predicting effective microRNA target sites in mammalian mRNAs. eLife 2015;4.
[39] Winek K, Lobentanzer S, Nadorp B, Dubnov S, Dames C, Jagdmann S, et al. Transfer RNA fragments replace microRNA regulators of the cholinergic poststroke immune blockade. Proc Natl Acad Sci U S A 2020;117(51):32606–16.
[40] Shulman D, Dubnov S, Zorbaz T, Madrer N, Paldor I, Bennett DA, et al. Sex-specific declines in cholinergic-targeting tRNA fragments in the nucleus accumbens in Alzheimer's disease. Alzheimers Dement 2023;19(11):5159–72.
[41] Venugopal SK, Jiang J, Kim TH, Li Y, Wang SS, Torok NJ, et al. Liver fibrosis causes downregulation of miRNA-150 and miRNA-194 in hepatic stellate cells, and their overexpression causes decreased stellate cell activation. Am J Physiol Gastrointest Liver Physiol 2010;298(1):G101–6.
[42] Wu JC, Chen R, Luo X, Li ZH, Luo SZ, Xu MY. MicroRNA-194 inactivates hepatic stellate cells and alleviates liver fibrosis by inhibiting AKT2. World J Gastroenterol 2019;25(31):4468–80.
[43] Aghajanzadeh T, Talkhabi M, Zali MR, Hatami B, Baghaei K. Diagnostic potential and pathogenic performance of circulating miR-146b, miR-194, and miR-214 in liver fibrosis. Noncoding RNA Res 2023;8(4):471–80.
[44] Torres LF, Cogliati B, Otton R. Green tea prevents NAFLD by modulation of miR-34a and miR-194 expression in a high-fat diet mouse model. Oxid Med Cell Longev 2019;2019:4168380.
[45] Zhu J, Cheng M, Zhao X. A tRNA-derived fragment (tRF-3001b) aggravates the development of nonalcoholic fatty liver disease by inhibiting autophagy. Life Sci 2020;257:118125.
[46] Huang P, Tu B, Liao HJ, Huang FZ, Li ZZ, Zhu KY, et al. Elevation of plasma tRNA fragments as a promising biomarker for liver fibrosis in nonalcoholic fatty liver disease. Sci Rep 2021;11(1):5886.
[47] Beenken A, Mohammadi M. The structural biology of the FGF19 subfamily. Adv Exp Med Biol 2012;728:1–24.
[48] Itoh N, Ornitz DM. Fibroblast growth factors: from molecular evolution to roles in development, metabolism and disease. J Biochem 2011;149(2):121–30.
[49] Kliewer SA, Mangelsdorf DJ. Bile acids as hormones: the FXR-FGF15/19 pathway. Dig Dis 2015;33(3):327–31.
[50] Dongiovanni P, Crudele A, Panera N, Romito I, Meroni M, De Stefanis C, et al. beta-Klotho gene variation is associated with liver damage in children with NAFLD. J Hepatol 2020;72(3):411–9.
[51] Somm E, Henry H, Bruce SJ, Bonnet N, Montandon SA, Niederländer NJ, et al. beta-Klotho deficiency shifts the gut-liver bile acid axis and induces hepatic alterations in mice. Am J Physiol Endocrinol Metab 2018;315(5):E833–47.
[52] Goodarzi H, Liu X, Nguyen HCB, Zhang S, Fish L, Tavazoie SF. Endogenous tRNA-derived fragments suppress breast cancer progression via YBX1 displacement. Cell 2015;161(4):790–802.
[53] Liu X, Mei W, Padmanaban V, Alwaseem H, Molina H, Passarelli MC, et al. A pro-metastatic tRNA fragment drives Nucleolin oligomerization and stabilization of its bound metabolic mRNAs. Mol Cell 2022;82(14):2604–2617 e8.
[54] Schneider CA, Rasband WS, Eliceiri KW. NIH Image to ImageJ: 25 years of image analysis. Nat Methods 2012;9(7):671–5.
[55] Dodt M, Roehr JT, Ahmed R, Dieterich C. FLEXBAR-flexible barcode and adapter processing for next-generation sequencing platforms. Biology 2012;1(3):895–905.
[56] Wang WC, Lin FM, Chang WC, Lin KY, Huang HD, Lin NS. miRExpress: analyzing high-throughput sequencing data for profiling microRNA expression. BMC Bioinform 2009;10:328.

[57] Friedlander MR, Mackowiak SD, Li N, Chen W, Rajewsky N. miRDeep2 accurately identifies known and hundreds of novel microRNA genes in seven animal clades. Nucleic Acids Res 2012;40(1):37–52.

[58] Loher P, Telonis AG, Rigoutsos I. MINTmap: fast and exhaustive profiling of nuclear and mitochondrial tRNA fragments from short RNA-seq data. Sci Rep 2017;7:41184.

[59] Langmead B, Salzberg SL. Fast gapped-read alignment with Bowtie 2. Nat Methods 2012;9(4):357–9.

[60] Dobin A, Davis CA, Schlesinger F, Drenkow J, Zaleski C, Jha S, et al. STAR: ultrafast universal RNA-seq aligner. Bioinformatics 2013;29(1):15–21.

[61] Anders S, Pyl PT, Huber W. HTSeq – a Python framework to work with high-throughput sequencing data. Bioinformatics 2015;31(2):166–9.

[62] Love MI, Huber W, Anders S. Moderated estimation of fold change and dispersion for RNA-seq data with DESeq2. Genome Biol 2014;15(12):550.

[63] Zhu A, Ibrahim JG, Love MI. Heavy-tailed prior distributions for sequence count data: removing the noise and preserving large differences. Bioinformatics 2019;35(12):2084–92.

